

$\text{Sr}_2\text{MgMoO}_{6-\delta}$ exhibits a lower η_a compared to $\text{Sr}_2\text{MnMoO}_{6-\delta}$. The dependence of η_a on the current density agrees well with that of the power density in Fig. 2. In addition, in most of the cases we observed, η_a is lower than the corresponding cathode overpotential, η_c . Here, LSCM exhibits a large η_a in H_2 and especially in $\text{H}_2/\text{H}_2\text{S}$, which shows that SMMO gives a superior performance.

Because the LDC buffer layer is also an MIEC that is catalytically active for fuel oxidation, a cell with only the LDC layer as anode and with Pt mesh and Pt paste as current collector was tested. The values of P_{max} were 528 and only 27 mW/cm^2 in dry H_2 and CH_4 , respectively, much lower than those of a cell with $\text{Sr}_2\text{MgMoO}_{6-\delta}$ as anode. Furthermore, EDS results for the $\text{Sr}_2\text{MgMoO}_{6-\delta}$ /LDC/LSGM/SCF cell after operating in H_2 , $\text{H}_2/\text{H}_2\text{S}$, and CH_4 for a total of 10 days showed no Pt in the LDC layer. This result demonstrates that the high performance of our cells with SMMO as anode was not dominated by the LDC layer. We further tried to use Au mesh and Au paste as the current collector. A drop in P_{max} occurred because of Au melting and a possible formation of Au-Mg alloy (21). In addition, because the $\text{Sr}_2\text{MgMoO}_{6-\delta}$ anode was poisoned by the existence of Au, the activity in CH_4 became very poor, which could not be improved by sputtering Pt on the anode surface. Instead, the observation reinforces the conclusion that SMMO

plays an important catalytic role in oxidation of CH_4 . We note that Pt paste is also catalytic for CH_4 oxidation. However, even without Pt paste, the $\text{Sr}_2\text{MgMoO}_{6-\delta}$ anode with buried Pt mesh as current collector still showed a P_{max} of 340 mW/cm^2 at 800°C in dry CH_4 .

With a 300- μm -thick LSGM electrolyte and SCF as the cathode, the double-perovskite anodes that we investigated show a high power density and a stable performance on power cycling. Moreover, they exhibit an excellent tolerance to sulfur. $\text{Sr}_2\text{MgMoO}_{6-\delta}$ also shows a very high power density in dry methane. Our results are also applicable to YSZ as electrolyte. These preliminary results indicate that optimization of the chemistry and the morphology of these double perovskites can provide an anode material for a SOFC that operates on natural gas.

References and Notes

1. B. A. Boukamp, *Nat. Mater.* **2**, 294 (2003).
2. A. Atkinson *et al.*, *Nat. Mater.* **3**, 17 (2004).
3. S. W. Tao, J. T. S. Irvine, *Nat. Mater.* **2**, 320 (2003).
4. S. W. Tao, J. T. S. Irvine, *J. Electrochem. Soc.* **151**, A252 (2004).
5. E. P. Murray, T. Tsai, S. A. Barnett, *Nature* **400**, 649 (1999).
6. Z. L. Zhan, S. A. Barnett, *Science* **308**, 844 (2005).
7. B. C. H. Steele, I. Kelly, H. Middleton, R. Rudkin, *Solid State Ionics* **28-30**, 1547 (1988).
8. A. L. Lee, R. F. Zabransky, W. J. Huber, *Ind. Eng. Chem. Res.* **29**, 766 (1990).
9. Y. Matsuzaki, I. Yasuta, *Solid State Ionics* **132**, 261 (2000).

10. X. J. Huang, W. Weppner, *J. Chem. Soc. Faraday Trans.* **92**, 2173 (1996).
11. S. W. Tao, J. T. S. Irvine, *J. Solid State Chem.* **165**, 12 (2002).
12. O. A. Marina, C. Bagger, S. Primdahl, M. Mogensen, *Solid State Ionics* **123**, 199 (1999).
13. S. Park, J. M. Vohs, R. J. Gorte, *Nature* **404**, 265 (2000).
14. S. A. Barnett, *Handbook of Fuel Cell Technology* (Wiley, Hoboken, NJ, 2003), vol. 4, p. 98.
15. H. P. He, R. J. Gorte, J. M. Vohs, *Electrochem. Solid-State Lett.* **8**, A279 (2005).
16. S. Zha, P. Tsang, Z. Cheng, M. Liu, *J. Solid State Chem.* **178**, 1844 (2005).
17. J. B. Goodenough, *Solid State Ionics* **26**, 87 (1988).
18. K. Q. Huang, J. B. Goodenough, *J. Alloys Compd.* **303-304**, 454 (2000).
19. K. Q. Huang, J. H. Wan, J. B. Goodenough, *J. Electrochem. Soc.* **148**, A788 (2001).
20. J. H. Wan, J. Q. Yan, J. B. Goodenough, *J. Electrochem. Soc.* **152**, A1511 (2005).
21. Details of the materials synthesis, characterization, fuel cell assembly, and performance are available as supporting material on Science Online.
22. We thank J. C. Denyszyn for assistance with the Labview 7.1 software, R. Caudillo for EDS measurement, J. S. Zhou for useful discussion on overpotentials, and the Robert A. Welch Foundation (Houston, TX) for support of this work.

Supporting Online Material

www.sciencemag.org/cgi/content/full/312/5771/254/DC1

Materials and Methods

Figs. S1 to S19

Tables S1 to S3

References

6 February 2006; accepted 13 March 2006

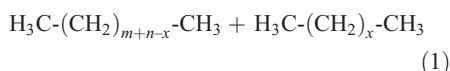
10.1126/science.1125877

Catalytic Alkane Metathesis by Tandem Alkane Dehydrogenation–Olefin Metathesis

Alan S. Goldman,^{1*} Amy H. Roy,² Zheng Huang,² Ritu Ahuja,¹ William Schinski,³ Maurice Brookhart^{2*}

With petroleum supplies dwindling, there is increasing interest in selective methods for transforming other carbon feedstocks into hydrocarbons suitable for transportation fuel. We report the development of highly productive, well-defined, tandem catalytic systems for the metathesis of *n*-alkanes. Each system comprises one molecular catalyst (a “pincer”-ligated iridium complex) that effects alkane dehydrogenation and olefin hydrogenation, plus a second catalyst (molecular or solid-phase) for olefin metathesis. The systems all show complete selectivity for linear (*n*-alkane) product. We report one example that achieves selectivity with respect to the distribution of product molecular weights, in which *n*-decane is the predominant high-molecular-weight product of the metathesis of two moles of *n*-hexane.

The interconversion of alkanes via alkane metathesis is a reaction with enormous potential applicability:



Alkanes are the major constituents of petroleum. As oil reserves dwindle, the world will increasingly rely on the Fischer-Tropsch pro-

cess (reductive oligomerization of CO and H_2) to produce liquid hydrocarbons—specifically *n*-alkanes—from the vast reserves of coal, natural gas, oil shale, and tar sands, or from biomass. The energy content of U.S. coal reserves alone, for example, is about 40 times that of U.S. petroleum reserves and is comparable to that of the entire world’s petroleum reserves (1).

Unfortunately, neither natural sources nor Fischer-Tropsch production yield alkane mixtures with a tightly controlled molecular weight (MW) distribution, which is important for varied

applications. For example, *n*-alkanes in the range of $\sim\text{C}_9$ to C_{20} constitute the ideal fuel for a diesel engine (which runs $\sim 30\%$ more efficiently than a gasoline engine); the absence of aromatic impurities results in cleaner burning than that of conventional diesel fuel or even gasoline (2, 3). *n*-Alkanes lower than $\sim\text{C}_9$, however, suffer from high volatility and lower ignition quality (cetane number) (4). In addition to F-T product mixtures, low-carbon number, low-MW alkanes are also major constituents of a variety of refinery and petrochemical streams. In general, there is currently no practical method for the interconversion of alkanes to give products of higher MW; this challenge provides extremely large-scale potential applications of alkane metathesis (Eq. 1). Additionally, Eq. 1 might be applied to the formation of low-MW products from high-MW reactants (e.g., by reaction with ethane). Although hydrocracking is already a well-established process for this purpose, Eq. 1 might offer an advan-

¹Department of Chemistry and Chemical Biology, Rutgers University, Piscataway, NJ 08854, USA. ²Department of Chemistry, University of North Carolina at Chapel Hill, Chapel Hill, NC 27599, USA. ³Chevron Research and Technology Co., 100 Chevron Way, Richmond, CA 94802, USA.

*To whom correspondence should be addressed. E-mail: agoldman@rutchem.rutgers.edu; brookhar@email.unc.edu

tage, for some applications, of higher selectivity and/or less severe conditions.

We report two systems in which the metathesis of linear alkanes is achieved efficiently and selectively at moderate temperatures via a tandem combination of two independent catalysts, one with activity for alkane dehydrogenation and the other for olefin metathesis. In particular, we exploit highly selective, soluble molecular catalysts developed for each of these reactions, as well as solid-phase olefin metathesis catalysts.

The basic tandem catalytic process is outlined in Fig. 1 for metathesis of an alkane of carbon number n (C_n) to give ethane and $C_{(2n-2)}$. A dehydrogenation catalyst, M , reacts with the alkane to give the corresponding C_n terminal alkene and MH_2 . Olefin metathesis of the 1-alkene generates ethylene and an internal $C_{(2n-2)}$ alkene. The alkenes thus produced serve as hydrogen acceptors and generate the two new alkanes via reaction with MH_2 , regenerating M and closing the catalytic cycle.

To date, two heterogeneous catalyst systems have been reported to effect the interconversion of alkanes. Burnett and Hughes showed that passage of butane over a mix of platinum on alumina (a dehydrogenation catalyst) and tungsten oxide on silica (an olefin metathesis catalyst) at high temperatures (399°C) results in formation of lower and higher MW alkanes, predominantly propane and pentane (24.7% and 15.9%, respectively, with 37.6% n -butane unreacted) (5, 6). In addition to linear saturated hydrocarbons, small quantities of branched C_4 and C_5 alkanes, methane, and alkenes were also formed. Supported Ta and W hydride catalysts that function as alkane metathesis catalysts at much lower temperatures were reported by Basset (7–9), but product yields were low. For example, a turnover number (mol of propane transformed per mol of catalyst) of 60 and conversion of 6% was observed for metathesis of propane to give C_1 to C_6 alkanes with the use of a supported Ta hydride species (120 hours, 150°C) (8). More recent work showed that an alumina-supported tungsten hydride species gave somewhat increased turnover numbers (8). Basset has shown that these systems operate via the reaction of metal centers with alkanes to give metal-carbene complexes (via α -H elimination) as well as free olefins (via β -H elimination and β -alkyl transfer) (10). Such pathways, unlike the one outlined in Fig. 1, are consistent with the reported formation, from linear alkanes, of both branched and linear products, as well as catalytic methane production (7–10).

Our investigation was largely based on the use of Ir-based pincer complexes, first reported by Jensen and Kaska (11, 12) and explored extensively in our own laboratories (13–17); specifically, complexes **1**, **2a**, and **2b** were used (Fig. 2). These systems exhibit high stability, but their dehydrogenation activity is inhibited by buildup of even moderate concen-

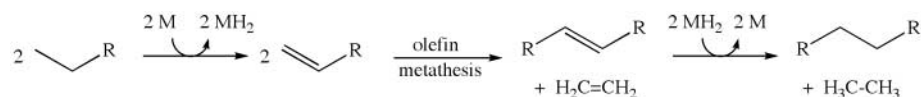


Fig. 1. Alkane metathesis via tandem transfer dehydrogenation–olefin metathesis illustrated with the formation and metathesis of two molecules of 1-alkene. M , active catalyst in the transfer dehydrogenation cycle [e.g., (pincer)Ir].

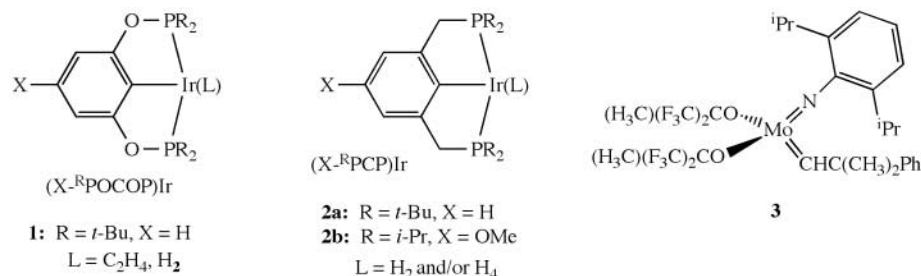


Fig. 2. Dehydrogenation catalysts **1** and **2** and Schrock-type metathesis catalyst **3**.

trations of alkene product. The dual catalytic system (Fig. 1) would require only a very low steady-state concentration of alkenes during catalysis; thus, inhibition of catalysis by product could be avoided. Numerous olefin metathesis catalysts are available (18–20); we examined the Schrock-type catalyst **3** (21, 22) after determining that the widely used Grubbs-type catalysts (19) react with and deactivate the iridium-based dehydrogenation catalysts.

Initial experiments combining **3** with Ir-based dehydrogenation catalysts in solution proved successful. An n -hexane solution containing 10 mM dehydrogenation catalyst precursor **1**- C_2H_4 (0.14 mol % relative to hexane) and 16 mM Schrock catalyst **3** was heated at 125°C under argon in a sealed glass vessel for 24 hours. This process converted 135 equivalents (relative to Ir) of n -hexane to a range of C_2 to C_{15} n -alkanes. No branched or cyclic alkanes were detected. Products were monitored by gas chromatography (GC) using mesitylene as an internal standard. The product distribution was concentrated in the C_2 to C_5 and C_7 to C_{10} ranges (Table 1, entry 1). Heating for longer times resulted in few additional turnovers. However, upon addition of more olefin metathesis catalyst **3**, alkane metathesis was reinitiated, indicating that decomposition of **3** is responsible for the deactivation of the system under these conditions. Using **1**- H_2 and two equivalents of t -butylethylene (TBE) as a hydrogen acceptor, along with catalyst **3**, similar results were obtained (Table 1, entry 2). [The reaction of the dihydride catalyst precursor **1**- H_2 with one equivalent of TBE is presumed to generate the catalytically active species (tBu POCOP)Ir (**1**). The use of two equivalents of TBE per mol of **1**- H_2 is expected to give results most comparable to those obtained with **1**- C_2H_4 , because **1**- C_2H_4 constitutes the same catalytically active species plus 1 mol of olefin.]

Controls were conducted, including experiments with (i) **1**- C_2H_4 and no metathesis catalyst; (ii) **2a**- H_2 and TBE, but with no metathesis catalyst; and (iii) metathesis catalyst **3**, but with no iridium-based catalyst. In none of these cases was any alkane metathesis observed after heating the n -hexane solutions for 24 hours at 125°C.

Pincer-ligated iridium complexes have been reported to dehydrogenate n -alkanes with high kinetic selectivity for the formation of the corresponding 1-alkene (15). Thus, the product distributions indicated in entries 1 and 2 in Table 1 presumably reflect a substantial degree of olefin isomerization before olefin metathesis under these conditions. For example, isomerization of 1-hexene to 2-hexene, followed by cross-metathesis between 2-hexene and 1-hexene, could give 1-pentene plus 2-heptene (Fig. 3) (18–20). Alternatively, or in addition, 5-decene (from the cross-metathesis of 2 mol of 1-hexene) could be isomerized to give 4-decene; metathesis with ethylene would then give 1-pentene and 1-heptene. The pincer-iridium complexes are well known to catalyze olefin isomerization (15). Thus, terminal dehydrogenation of n -hexane in tandem with olefin metathesis, when coupled with rapid olefin isomerization, can account for the C_3 to C_5 and C_7 to C_9 alkanes (Fig. 3).

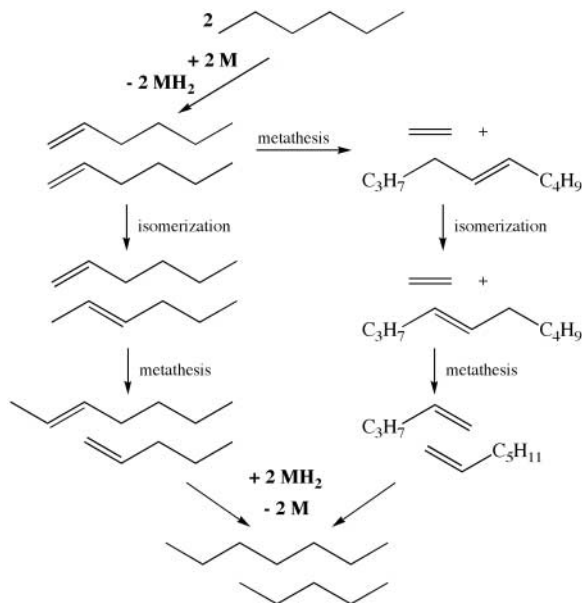
Alkanes with carbon number greater than 10, produced from hexane, must derive from olefin metathesis of at least one alkene of $C_{n>6}$. The $C_{n>6}$ alkene may result from dehydrogenation of the corresponding n -alkane primary product, or it may be obtained directly via cross-metathesis of hexenes, before the resulting olefin (e.g., 5-decene) is hydrogenated.

Consistent with the hypothesis that 1-alkenes are the initial dehydrogenation products, under certain conditions n -decane is the major heavy ($C_{n>6}$) product of n -hexane metathesis (the non-degenerate cross-metathesis of 1-hexene can

Table 1. Representative examples of the metathesis of *n*-hexane (7.6 M) by **1** or **2** (10 mM) and **3** (16 mM): distribution of C₂ to C₁₅ *n*-alkane products.

Entry	Ir catalyst	[TBE] (mM)	Temp. (°C)	Time	Product concentration (mM)												Total product (M)	
					C ₂	C ₃	C ₄	C ₅	C ₇	C ₈	C ₉	C ₁₀	C ₁₁	C ₁₂	C ₁₃	C ₁₄		C _{≥15}
1	1 -C ₂ H ₄	0	125	6 hours	123	105	183	131	73	70	47	10	4	2	1	0.3	0.75	
				24 hours	233	191	319	234	133	122	81	22	9	5	2	1	1.35	
				2 days	261	215	362	265	147	138	89	25	11	6	3	1	1.52	
				4 days	264	218	372	276	154	146	95	26	12	6	3	1	1.57	
				Added additional 3 (8 mM)														
				5 days	502	436	721	420	239	223	153	56	30	18	10	5	2.81	
2	1 -H ₂	20	125	1 day	458	345	547	258	151	139	95	29	13	6	3	2	2.05	
3	2a -H ₂ *	20	125	23 hours	(131)	176	127	306	155	37	49	232	18	4	4	10	2	1.25
				Added additional 3 (6.4 mM)														
				46 hours	(189)	255	193	399	208	61	81	343	31	9	9	22	7	1.81

*6.4 mM catalyst **3** added initially. Ethane concentrations for entry 3 are extrapolated as explained in the text. For entries 1 and 2, no separation of C₂ and C₃ peaks was obtained (values shown are not extrapolated).

Fig. 3. Two possible pathways for the metathesis of *n*-hexane to give *n*-pentane and *n*-heptane, initiated by dehydrogenation at the *n*-hexane terminal position.**Table 2.** Concentrations of C₂ to C₃₈ *n*-alkane products resulting from the metathesis of *n*-hexane (4.36 M) and eicosane (*n*-C₂₀H₄₂; 1.09 M) by **1**-C₂H₄ (7.14 mM) and **3** (11.43 mM) at 125°C.

Time	Product concentration (M)						Total product
	C ₂₋₅	C ₇₋₁₀	C ₁₁₋₁₄	C ₁₅₋₁₉	C ₂₁₋₂₄	C ₂₅₋₃₈	
1 day	0.44	0.36	0.24	0.31	0.14	0.066	1.56
6 days	0.56	0.64	0.31	0.27	0.12	0.070	1.97

only yield ethene and 5-decene). Combining dehydrogenation catalyst **2a** and metathesis catalyst **3** (Table 1, entry 3) leads to this outcome. (The formation of *n*-tetradecane presumably results from the secondary metathesis reaction of *n*-decane with *n*-hexane.) Presumably, under the conditions of this reaction, diphosphine-ligated **2a** catalyzes isomerization more slowly (or more slowly relative to hydrogenation) than does the diphosphinite-ligated species **1**. This reaction was also monitored by ¹³C nuclear magnetic resonance spectroscopy (NMR), a method that yields less precise results

than GC but facilitates continuous monitoring in a sealed reaction vessel. The NMR results were generally consistent with those obtained by GC, and in particular they revealed that the ratio of the major *n*-alkane products did not considerably change with time.

Although it is difficult to precisely quantify ethane production under our conditions, the solution concentration for the first run in entry 3 was measured by GC as 128 mM. GC analysis of the gas phase indicated the presence of 1.7 μmol of ethane; if this quantity were also in solution, the total ethane concentration would

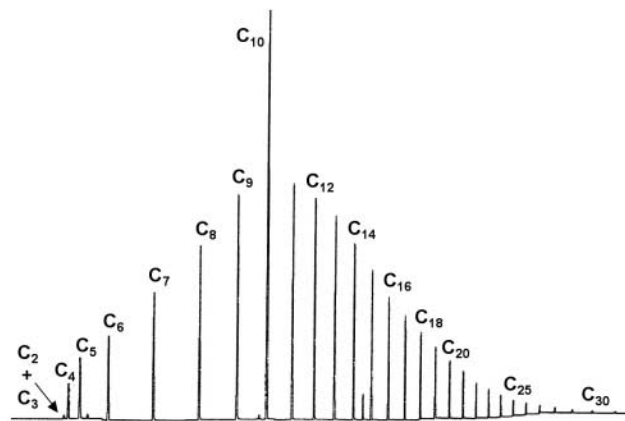
have been 131 mM. (Likewise, a small amount of propane in the gas phase brings the effective concentration from 175 mM to 176 mM.) The average carbon number of all products was found to be ~6.0 (measured as 5.95), an indication that no significant loss of lighter alkanes had occurred (which would raise the observed value above 6.0). The “effective ethane concentration” of 131 mM is substantially lower than the concentration of *n*-decane observed (232 mM). This discrepancy between ethane and *n*-decane production is probably largely attributable to secondary metathesis of the ethene product with 2- or 3-hexenes (which would then contribute to the formation of propene, butene, and pentene). It is also worth noting in the context of this experiment that only trace quantities of methane were observed [0.5 mM effective concentration, probably formed via decomposition of the expected molybdenum methylidene intermediate (18–20)]. This result contrasts sharply with the Basset systems, in which methane is formed catalytically; this difference is in accord with the key role played by α-H elimination and β-alkyl elimination in the Basset systems (7–10). The catalytic cycle in the systems reported here does not involve either of these elimination steps.

In addition to the alkane disproportionation (self-metathesis) illustrated above, the catalyst system may be used for alkane comproportionation (cross-metathesis)—that is, the production of intermediate-MW alkanes from low-MW and high-MW reactants. Table 2 shows the result of treating a mixture of 4:1 (mol:mol) *n*-hexane and the C₂₀ alkane, *n*-eicosane, with catalysts **1** and **3**.

Monitoring the reactions by NMR spectroscopy affords insight into the resting state(s) of the catalysts as well as the extent of alkane metathesis. ³¹P and ¹H NMR spectroscopy indicates that some loss of catalyst **2a**-H₂ occurs during the reaction of *n*-hexane solution. However, a substantial concentration of **2a**-H₂ remains, even when the reaction is no longer progressing. The olefin metathesis catalyst is less

Table 3. Distribution of C₂ to C₃₄ *n*-alkane products from the metathesis of *n*-decane (5.1 M) by Ir-based catalysts (9.0 to 9.5 mM) and Re₂O₇/Al₂O₃ (16 mM effective Re₂O₇ concentration) at 175°C.

Ir catalyst	[TBE] (mM)	Time	<i>n</i> -Alkane concentration (mM)																	Total product (M)	
			C ₂	C ₃	C ₄	C ₅	C ₆	C ₇	C ₈	C ₉	C ₁₀	C ₁₁	C ₁₂	C ₁₃	C ₁₄	C ₁₅	C ₁₆	C ₁₇	C ₁₈		[>C ₁₈]
1-C ₂ H ₄ (9.5 mM)	0	3 hours	3.9	2.8	8.3	10	12	12	13	16	4980	15	11	9.3	7.2	6.0	4.6	2.1	1.3	1.9	0.14
		18 hours	5.4	9.7	39	43	43	48	55	64	4580	61	46	38	28	23	17	6.9	3.7	5.4	0.54
		7 days	26	101	117	118	115	140	163	3760	154	115	94	71	58	43	18	9.8	16.3	1.36	
2a-H ₂ (9.0 mM)	18	3 hours	16	61	86	98	122	142	152	3990	137	104	78	53	37	23	9.3	5.2	6.3	1.13	
		11 days	39	207	299	327	382	427	446	1500	408	314	245	174	129	87	48	32	58	3.62	
2b-H ₄ (9.1 mM)	35	3 hours	15	81	117	134	146	172	181	3490	177	147	120	91	72	52	34	26	63	1.63	
		18 hours	39	160	234	265	280	318	324	1870	317	271	226	176	145	110	76	61	194	3.20	
		9 days	44	220	332	346	405	456	457	753	429	362	300	233	195	151	108	88	241	4.37	

Fig. 4. GC trace of product mixture resulting from the metathesis of *n*-decane (solvent) by 2b-H₄ and Re₂O₇/Al₂O₃ after 9 days at 175°C (see Table 3).

easily monitored because its resting state depends on the nature of the olefins present in solution; the loss of the 2-methyl-2-phenylpropylidene ligand and the expected formation of 2-methyl-2-phenylbutane (resulting from hydrogenation of 3-methyl-3-phenylbutene) are observed early in the course of the reaction. However, the appearance of free 2,6-diisopropylaniline is observed to approximately coincide with the decreased reaction rate; thus, decomposition of **3** appears to be an important factor limiting turnover numbers in this case. This conclusion is in accord with the experiments in which addition of **3** reinitiates catalytic activity.

In contrast to (^tBuPCP)Ir-based 2a-H₂, the resting state of the (^tBuPOCOP)Ir-based catalysts (**1**) is the Ir(I)(alkene) complex. For example, monitoring by ³¹P NMR spectroscopy of *n*-hexane metathesis by 1-C₂H₄ and **3** indicates that at early stages of the reaction (~150 min), 1-C₂H₄ is the major Ir resting state, with 1-(1-propene), 1-(1-butene), 1-(1-pentene), 1-(1-hexene), and 1-(internal-hexene) present in small concentrations. However, at later stages of the reaction (4 days), 1-(1-hexene) is observed as the major iridium species in solution. The resting state of the Ir species appears to reflect the activity of the metathesis catalyst. Because the metathesis catalyst decays at the late stage of the reaction, ethylene is no longer produced, although it continues to be

consumed as a hydrogen acceptor. As a result, the dehydrogenation of hexane results in the gradual conversion of 1-C₂H₄ to 1-(1-hexene).

Given the instability of the molybdenum alkylidene catalysts, we turned to investigation of the supported Re metathesis catalyst Re₂O₇/Al₂O₃, which exhibits greater stability at high temperatures (23). Reactions were conducted at 175°C with *n*-decane as the solvent/substrate (Table 3) (24). (Control experiments with Re₂O₇/Al₂O₃, with no iridium catalyst present, gave no alkane metathesis after 3 days at 175°C.) The (PCP)Ir catalysts (**2**) proved more effective than the (POCOP)Ir systems (**1**). In a typical experiment, an *n*-decane (2.5 ml, 12.8 mmol) solution of 2b-H₄ (12.8 mg, 0.0227 mmol), TBE (10 μl, 0.078 mmol), and hexamethylbenzene (10 mg, internal standard) was heated over Re₂O₇/Al₂O₃ (535 mg, 3 wt % Re₂O₇) at 175°C under argon and monitored by GC. After 3 hours, C₂ to C₂₈ alkanes were observed with total product concentration estimated at 1.6 M (corresponding to 180 mol of product per mol of Ir). Catalysis slowed, but after 9 days, product concentrations reached 4.4 M. Remarkably, at 9 days, the *n*-decane starting material was comparable in molar quantity to *n*-nonane and *n*-undecane products, with measured C₉:C₁₀:C₁₁ molar ratios of 0.6:1:0.6 (Table 3 and Fig. 4).

Because decomposition of the olefin metathesis catalysts appears to limit conversions,

we expect that more robust olefin metathesis catalysts will yield higher turnover numbers in future studies. We also expect that more active dehydrogenation catalysts will give more turnovers before decomposition of the metathesis catalyst, and that catalysts that are less prone to isomerize the olefin intermediates will yield greater selectivity for C_(2*n*-2) products. The nature of the tandem system permits the detailed investigation of the component catalysts individually, and the development of more suitable catalysts for both dehydrogenation and olefin metathesis (25) is under way.

References and Notes

- O. Levenspiel, *Ind. Eng. Chem. Res.* **44**, 5073 (2005).
- M. E. Dry, *J. Chem. Technol. Biotechnol.* **77**, 43 (2001).
- J. P. Szybist, S. R. Kirby, A. L. Boehman, *Energy Fuels* **19**, 1484 (2005).
- M. J. Murphy, J. D. Taylor, R. L. McCormick, *Compendium of Experimental Cetane Number Data* (National Renewable Energy Laboratory, Golden, CO, 2004) (www.nrel.gov/vehiclesandfuels/pdfs/sr368051.pdf).
- R. L. Burnett, T. R. Hughes, *J. Catal.* **31**, 55 (1973).
- References to earlier related patent work are contained in (5).
- J. M. Basset *et al.*, *J. Am. Chem. Soc.* **127**, 8604 (2005).
- E. L. Roux *et al.*, *Angew. Chem. Int. Ed.* **44**, 6755 (2005).
- V. Vidal, A. Theolier, J. Thivolle-Cazat, J.-M. Basset, *Science* **276**, 99 (1997).
- C. Thieuleux *et al.*, *J. Mol. Catal. A* **213**, 47 (2004).
- M. Gupta, C. Hagen, R. J. Flesher, W. C. Kaska, C. M. Jensen, *Chem. Commun.* **1996**, 2083 (1996).
- M. Gupta, C. Hagen, W. C. Kaska, R. E. Cramer, C. M. Jensen, *J. Am. Chem. Soc.* **119**, 840 (1997).
- I. Göttker-Schnetmann, P. White, M. Brookhart, *J. Am. Chem. Soc.* **126**, 1804 (2004).
- I. Göttker-Schnetmann, M. Brookhart, *J. Am. Chem. Soc.* **126**, 9330 (2004).
- F. Liu, E. B. Pak, B. Singh, C. M. Jensen, A. S. Goldman, *J. Am. Chem. Soc.* **121**, 4086 (1999).
- W. Xu *et al.*, *Chem. Commun.* **1997**, 2273 (1997).
- K. Zhu, P. D. Achord, X. Zhang, K. Krogh-Jespersen, A. S. Goldman, *J. Am. Chem. Soc.* **126**, 13044 (2004).
- D. Astruc, *N. J. Chem.* **29**, 42 (2005).
- R. H. Grubbs, *Tetrahedron* **60**, 7117 (2004).
- R. R. Schrock, A. H. Hoveyda, *Angew. Chem. Int. Ed.* **42**, 4592 (2003).
- R. R. Schrock, *Chem. Commun.* **2005**, 2773 (2005).
- R. R. Schrock *et al.*, *J. Am. Chem. Soc.* **112**, 3875 (1990).
- C. Pariya, K. N. Jayaprakash, A. Sarkar, *Coord. Chem. Rev.* **168**, 1 (1998).
- The iridium-based dehydrogenation catalysts appear to be adsorbed on alumina. Accordingly, when alumina is treated with alkane solutions of the iridium complexes, the solutions turn colorless and the support acquires the red color of the catalyst. However, we have yet to

determine whether dehydrogenation is actually catalyzed by supported-phase iridium complexes, or whether it is effected by a low concentration of catalyst that may slowly leach into solution.

25. S. Scott *et al.*, in *Abstracts of Papers, 229th ACS National Meeting* (American Chemical Society, Washington, DC, 2005), abstract PETR-022.

26. This material is based on work supported by NSF under the auspices of the Center for the Activation and Transformation of Strong Bonds, grant CHE-0434568.

Supporting Online Material

www.sciencemag.org/cgi/content/full/312/5771/257/DC1
Materials and Methods

Figs. S1 and S2
References

13 December 2005; accepted 3 March 2006
10.1126/science.1123787

High Natural Aerosol Loading over Boreal Forests

P. Tunved,^{1*} H.-C. Hansson,¹ V.-M. Kerminen,² J. Ström,¹ M. Dal Maso,³ H. Lihavainen,² Y. Viisanen,² P. P. Aalto,³ M. Komppula,² M. Kulmala³

Aerosols play a key role in the radiation balance of the atmosphere. Here, we present evidence that the European boreal region is a substantial source of both aerosol mass and aerosol number. The investigation supplies a straightforward relation between emissions of monoterpenes and gas-to-particle formation over regions substantially lacking in anthropogenic aerosol sources. Our results show that the forest provides an aerosol population of 1000 to 2000 particles of climatically active sizes per cubic centimeter during the late spring to early fall period. This has important implications for radiation budget estimates and relevancy for the evaluation of feedback loops believed to determine our future climate.

The boreal forest plays an important role in both climate regulation and carbon cycling (1–3). Boreal forests represent one-third of all forested land and cover 15 million square kilometers of land. The boreal region is characterized by large seasonal variations in temperature, and the flora is dominated by different pine and spruce species. Most boreal forests contain few large sources of anthropogenic pollution.

In the northern European boreal region, long-term studies of aerosol formation and transformation processes have been performed at several measurement sites. One of the major research aims of these studies, including those performed at the Finnish background station Hyytiälä (4–7), has been to investigate the role of particle formation. This is important because homogeneous or ion-induced nucleation can provide substantial numbers of aerosols in an environment otherwise deficient of primary sources contributing to the fine-particle mode. This has clear relevance for understanding radiation budgets. Similar issues have been addressed at other locations in northern Europe. Particle-formation events over the boreal forest are well-studied phenomena at stations located in Finnish Lapland [Pallas and Värriö (8–10)] and at the Scandinavian rim of the boreal region in Sweden [Aspvreten (11)]. The mechanisms responsible for the formation and growth

of these particles are still uncertain. Although sulfuric acid is one of the most likely candidates thought to be responsible for the formation of the initial nanometer-sized particles, sulfur chemistry does not sustain enough sulfuric acid in the atmosphere to explain more than a small fraction of the observed particle-size growth rate. To explain the observed growth, which is up to a diameter of 50 to 100 nm, other compounds are required (12).

Organic constituents comprise a large fraction of the global aerosol burden (13, 14) and there is growing evidence that naturally emitted terpenes contribute notably to gas-to-particle formation (15). In the boreal region of northern Europe, monoterpenes are abundant at concentrations ranging from some tens of parts per trillion up to parts per billion depending on season, boundary layer conditions, and temperature (16–18). When released into the atmo-

sphere, monoterpenes undergo oxidation by ozone, hydroxyl radical, and nitrate radical to yield numerous compounds, the most interesting of which are oxygenated carbon compounds such as mono- and dicarboxylic acids (19). Similar compounds may contribute considerably, either directly or through polymerization in the particle phase (20), to the gas-to-particle conversion rate over forested areas.

Here, we present evidence of substantial contributions to the aerosol mass and abundance from natural emissions of aerosol precursor gases, most likely terpenes. The approach utilizes a statistical method including long-term observations of the submicrometer aerosol number-size distribution at three different stations in the Finnish boreal zone. The three locations selected for this purpose are the station for Measuring Forest Ecosystem-Atmosphere Relations (SMEAR I) located at Värriö [67°46'N, 29°35'E, 390 m above sea level (asl)], the Pallas-Sodankylä Global Atmospheric Watch (GAW) station located close to Pallas (68°01'N, 24°10'E, 303 m asl), and the SMEAR II station (Hyytiälä, 61°51'N, 24°17'E, 170 m asl). The database used includes 5 years (1999 to 2004) of aerosol number-size distribution data from the stations. The study considers only the period from April to September.

The current ambition is to investigate the characteristic changes of the aerosol population in air masses undergoing marine to continental transition over forested areas in northern Norway, Sweden, and Finland. Previous investigations (11, 21) have shown that substantial sources affect the aerosol during this transition. However, these investigations only account for a

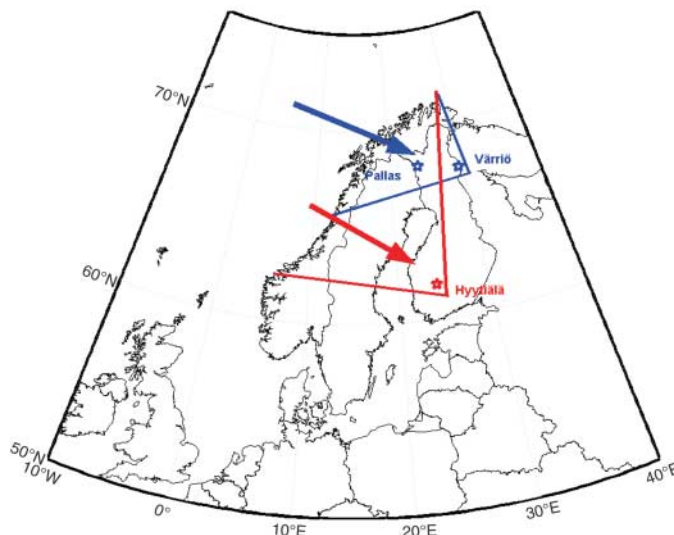


Fig. 1. The transport sectors of the trajectories used in the study. To qualify, each trajectory must spend 90% of the time in the sector. The selection of sectors assures minimum input from anthropogenic sources. The northerly stations share the same sector. Red, Hyytiälä; blue, Värriö and Pallas.

¹Department of Applied Environmental Science (ITM), Air Pollution Laboratory, Frescativägen 54, SE-106 91, Stockholm, Sweden. ²Finnish Meteorological Institute, Post Office Box 503 (Erik Palmenin Aukio 1), FI-00101 Helsinki, Finland. ³Department of Physical Sciences, University of Helsinki, Gustav Hällströmin katu 2, FI-00014 Helsinki, Finland.

*To whom correspondence should be addressed. E-mail: peter.tunved@itm.su.se